J|A|C|S ARTICLES

Published on Web 12/30/2008

Synthesis of an Electromagnetic Wave Absorber for High-Speed Wireless Communication

Asuka Namai,[†] Shunsuke Sakurai,[†] Makoto Nakajima,[‡] Tohru Suemoto,[‡] Kazuyuki Matsumoto,[§] Masahiro Goto,[§] Shinya Sasaki,[§] and Shin-ichi Ohkoshi*,[†]

Department of Chemistry, School of Science, The University of Tokyo, 7-3-1 Hongo, Bunkyo-ku, Tokyo 113-0033, Japan, Institute for Solid State Physics, The University of Tokyo, 5-1-5 Kashiwanoha, Kashiwa, Chiba 277-8581, Japan, and Dowa Electronics Materials Co., Ltd., 1-3-1 Kaigandori, Okayama 702-8506, Japan

Received October 8, 2008; E-mail: ohkoshi@chem.s.u-tokyo.ac.jp

Abstract: Millimeter waves (30−300 GHz) are starting to be used in next generation high-speed wireless communications. To avoid electromagnetic interference in this wireless communication, finding a suitable electromagnetic wave absorber in the millimeter wave range is an urgent matter. In this work, we prepared a high-performance millimeter wave absorber composed of a series of aluminum-substituted ε-iron oxide, ε-$Al_xFe_{2-x}O_3$, nanomagnets ($0 \le x \le 0.40$) with a particle size between 25 and 50 nm. The materials in this series have an orthorhombic crystal structure in the $Pna2_1$ space group, which has four nonequivalent Fe sites and Al ion that predominantly occupies the tetrahedral [FeO_4] site. The field-cooled magnetization curves showed that the T_C values were 448, 480, and 500 K for $x = 0.40$, 0.21, and 0, respectively. The magnetization versus external magnetic field showed that the coercive field H_c values at 300 K were 10.2, 14.9, and 22.5 kOe for $x = 0.40$, 0.21, and 0, respectively. The millimeter wave absorption properties were measured at room temperature by terahertz time domain spectroscopy. The frequencies of the absorption peaks for $x = 0.40$, 0.30, 0.21, 0.09, 0.06, and 0 were observed at 112, 125, 145, 162, 172, and 182 GHz, respectively. These absorptions are due to the natural resonance achieved by the large magnetic anisotropies in this series. Such frequencies are the highest ones for magnetic materials. Because aluminum is the third most abundant atom, aluminum-substituted ε-iron oxide is very economical, and thus these materials are advantageous for industrial applications.

Introduction

To avoid potential health effects from high exposure to electromagnetic (EM) waves, unnecessary EM waves should be eliminated to protect human bodies, especially expectant mothers and children.[1] In addition, electromagnetic interference (EMI) is a fatal problem in wireless communication. Recently, due to the marvelous development of transistors composed of complementary metal−oxide semiconductors or double heterojunction bipolar transistors,[2−6] EM waves in the millimeter wave range are beginning to be used in next generation electronic devices for high-speed wireless communication.[7−9] To prevent potential health effects and the EMI problem in this wireless communication, a millimeter wave absorber must be equipped on electronic devices as an isolator[10−13] and should be painted on objects. Hence, finding a suitable magnetic absorber is a matter of urgency. In general, when an EM wave is irradiated into a ferromagnet, the gyromagnetic effect leads to resonance, which is called a "natural resonance" as shown in Figure 1.[14−17] The natural resonance frequency (f_r) is proportional to the magnetocrystalline anisotropy field (H_a), which is expressed by

[†] Department of Chemistry, The University of Tokyo.
[‡] Institute for Solid State Physics, The University of Tokyo.
[§] Dowa Electronics Materials. Co.

(1) Committee on identification of research needs relating to potential biological or adverse health effects of wireless communications devices, National Research Council. *Identification of Research Needs Relating to Potential Biological or Adverse Health Effects of Wireless Communication*; National Academies Press: WA, 2008.
(2) Doan, C. H.; Emami, S.; Niknejad, A. M.; Brodersen, R. W. *IEEE J. Solid-State Circuits* **2005**, *40*, 144–155.
(3) Rodwell, M. J. W. *High Speed Integrated Circuit Technology, towards 100 GHz Logic*; World Scientific: Singapore, 2001.
(4) Cao, C.; Seok, E. Y.; O, K. K. *IEE Electron. Lett.* **2006**, *42*−*4*, 208–210.
(5) Wu, B. R.; Snodgrass, W.; Feng, M.; Cheng, K. Y. *J. Cryst. Growth* **2007**, *301*−*302*, 1005–1008.
(6) Snodgrass, W.; Wu, B. R.; Hafez, W.; Cheng, K. Y.; Feng, M. *Appl. Phys. Lett.* **2006**, *88*, 222101.
(7) Vinoy, K. J.; Jha, R. M. *Radar Absorbing Materials*; Kluwer: Boston, 1996.
(8) Vilcot, A.; Cabon, B.; Chazelas, J. *Microwave Photonics*; Kluwer: Boston, 1996.
(9) Naito, Y.; Suetake, K. *IEEE Trans. Microwave Theory Tech.* **1971**, *19*, 65–72.
(10) Lacheisserie, E. T.; Gignoux, D.; Schlenker, M. *Magnetism*; Kluwer: Dordrecht, 2002.
(11) Wohlfarth, E. P. *Handbook of Magnetic Materials*; Elsevier: Amsterdam, 1980; Vol. 2.
(12) Zhou, Z. G. *Magnetic Ferrite Materials*; Science Press: Beijing, 1981.
(13) Matsumoto, K.; Kondo, A.; Habu, T.; Hayashi, K.; Hashimoto, O. *Microwave Opt. Tech. Lett.* **2006**, *48*, 2065–2067.
(14) Chikazumi, S. *Physics of Ferromagnetism*; Oxford University Press: New York, 1997.
(15) Snoek, J. L. *Physica* **1948**, *14*, 207–217.
(16) Yoshida, S.; Sato, M.; Sugawara, E.; Shimada, Y. *J. Appl. Phys.* **1999**, *85*, 4636–4638.
(17) Ohkoshi, S.; Kuroki, S.; Sakurai, S.; Matsumoto, K.; Sato, K.; Sasaki, S. *Angew. Chem., Int. Ed.* **2007**, *46*, 8392–8395.

 10.1021/ja807943v CCC: $40.75

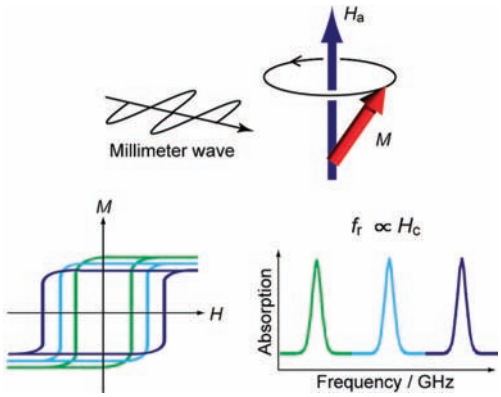

Figure 1. Schematic illustration of natural resonance due to the gyromagnetic effect. Precession of magnetization (M) around an anisotropy field (H_a) causes electromagnetic wave absorption. Natural resonance frequency (f_r) is expressed as $f_r = (\nu/2\pi)H_a$. In magnets with a uniaxial magnetic anisotropy, f_r is proportional to coercive field (H_c).

$f_r = (\nu/2\pi)H_a$, where ν is the gyromagnetic ratio. In this work, we prepared a high-performance millimeter wave absorber composed of a series of ε-$Al_xFe_{2-x}O_3$ nanomagnets. These magnetic materials show natural resonances in the region up to 182 GHz, which is the highest frequency for magnetic materials. Because aluminum is the third most abundant atom, production costs are very economical, which is very attractive for practical applications.

Experimental Section

The samples for $x = 0.06$, 0.09, 0.21, 0.30, and 0.40 were prepared by combining reverse-micelle and sol−gel techniques. Microemulsion systems were formed by $C_{16}H_{33}N(CH_3)_3Br$ and $CH_3(CH_2)_3OH$ in $CH_3(CH_2)_6CH_3$ with a molar ratio of $[H_2O]/[C_{16}H_{33}N(CH_3)_3Br] = 31$. The microemulsion containing an aqueous solution of $Fe(NO_3)_3$ (0.49, 0.48, 0.45, 0.43, and 0.38 mol dm^{-3} for $x = 0.06$, 0.09, 0.21, 0.30, and 0.40, respectively) and $Al(NO_3)_3$ (0.013, 0.025, 0.050, 0.075, and 0.125 mol dm^{-3} for $x = 0.06$, 0.09, 0.21, 0.30, and 0.40, respectively) was mixed with another microemulsion containing 5 mol dm^{-3} NH_3 aqueous solution while rapidly stirring. $Si(C_2H_5O)_4$ was then added into the solution to yield a final molar ratio of $[Si]/[Fe + Al] = 1.5$. This mixture was stirred for 20 h, and the materials were subsequently sintered for 4 h in air. The annealing temperature of $x = 0.21$ was 1025 °C, whereas the annealing temperature of $x = 0.06$, 0.09, 0.30, and 0.40 was 1050 °C. The SiO_2 matrices were etched by a NaOH solution for 24 h at 60 °C. The sample for $x = 0$ was prepared by an impregnation method based on mesoporous silica nanoparticles. Mesoporous silica nanoparticles were synthesized by a method similar to that reported by Möller et al.[18] First, 62 mmol of $Si(C_2H_5O)_4$ was added into a solution composed of 4 mol of H_2O, 0.18 mol of C_2H_5OH, 16 mmol of $C_{16}H_{33}N(CH_3)_3Cl$, and 62 mmol of $N(CH_2CH_2OH)_3$ at 60 °C, and stirred for 2 h. Mesoporous silica nanoparticles were obtained after centrifuging and heating at 600 °C. A methanol and water solution containing 1.25 mmol of $Fe(NO_3)_3$ was immersed into 11.7 mmol of mesoporous silica, and heated in air at 1200 °C for 4 h. The SiO_2 matrices were etched by a NaOH solution for 24 h at 70 °C.

Elemental analyses of the prepared samples were performed using inductively coupled plasma mass spectroscopy (ICP-MS, Agilent Technologies, HP 4500). The transmission electron microscopy (TEM) measurements were conducted using a JEOL JEM-2000EXII, while the X-ray diffraction (XRD) measurements were

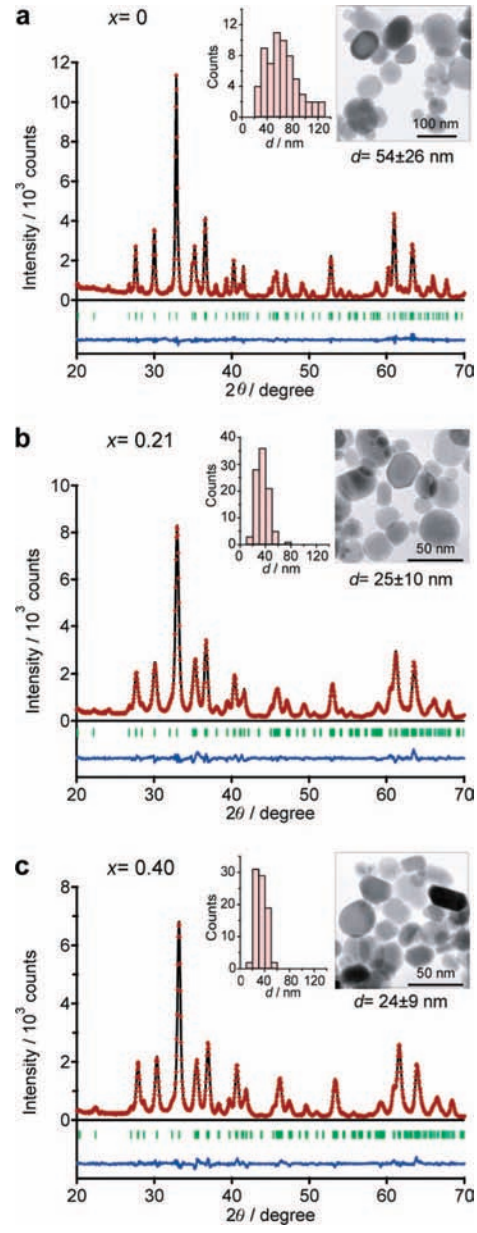

Figure 2. Powder X-ray diffraction patterns in ε-$Al_xFe_{2-x}O_3$ for (a) $x = 0$, (b) $x = 0.21$, and (c) $x = 0.40$. Red dots, black lines, and blue lines are the observed patterns, calculated patterns, and their differences, respectively. Green bars represent the calculated positions of the Bragg reflections of ε-$Al_xFe_{2-x}O_3$. Insets are TEM images and the distribution of particle size (d).

conducted by a Rigaku RINT2100 with Cu Kα radiation (λ = 1.5418 Å) at 289 K within the range of $10° \le 2\theta \le 100°$. Rietveld analyses were performed by the RIETAN-FP program.[19] The magnetic properties were measured using a superconducting quantum interference device (SQUID) magnetometer (Quantum Design, MPMS 7).

For terahertz (THz) time domain spectroscopy measurements, a pump−probe measurement system was used.[20] Figure S1 in the Supporting Information shows a schematic diagram of the THz time domain spectroscopy system. The output of a mode-locked Ti: sapphire femtosecond pulse laser with a time duration of 20 fs at a repetition rate of 76 MHz was divided into a pump and probe beam. As a THz wave emitter and detector, dipole type and bow-

(18) Möller, K.; Kobler, J.; Bein, T. *Adv. Funct. Mater.* **2007**, *17*, 605–612.
(19) Izumi, F.; Momma, K. *Solid. State Phenom.* **2007**, *130*, 15–20.
(20) Sakai, K. *Terahertz Optoelectronics*; Springer-Verlag: Berlin, 2005.

Table 1. Crystal Structure Parameters of ε-$Al_xFe_{2-x}O_3$ at Room Temperature Obtained by Rietveld Refinement of the X-ray Diffraction Patterns[a]

		$x = 0$	$x = 0.06$	$x = 0.09$	$x = 0.21$	$x = 0.30$	$x = 0.40$
a (Å)		5.0935 (2)	5.0873 (3)	5.0846 (2)	5.0771 (3)	5.0693 (3)	5.0432 (3)
b (Å)		8.7880 (3)	8.7768 (6)	8.7659 (5)	8.7520 (7)	8.7295 (6)	8.6776 (5)
c (Å)		9.4758 (3)	9.4694 (5)	9.4576 (5)	9.4405 (6)	9.4155 (6)	9.3585 (4)
V (Å^3)		424.15 (3)	422.82 (4)	421.53 (4)	419.49 (5)	416.66 (5)	409.55 (4)
R_{wp} (%)		6.71	6.76	6.78	6.25	7.09	6.48
S		1.53	1.37	1.35	1.70	1.52	1.35
Al occupancy (%)	A	0	3 (3)	3 (3)	0 (4)	10 (2)	12 (2)
	B	0	0 (4)	−1 (4)	3 (2)	2 (1)	1 (1)
	C	0	−2 (1)	−1 (1)	8 (2)	11 (1)	14 (1)
	D	0	11 (2)	17 (3)	30 (5)	38 (3)	52 (2)

[a] All samples are in the $Pna2_1$ space group. Data include the lattice parameters and Al substitution rates of Fe sites (A−D).

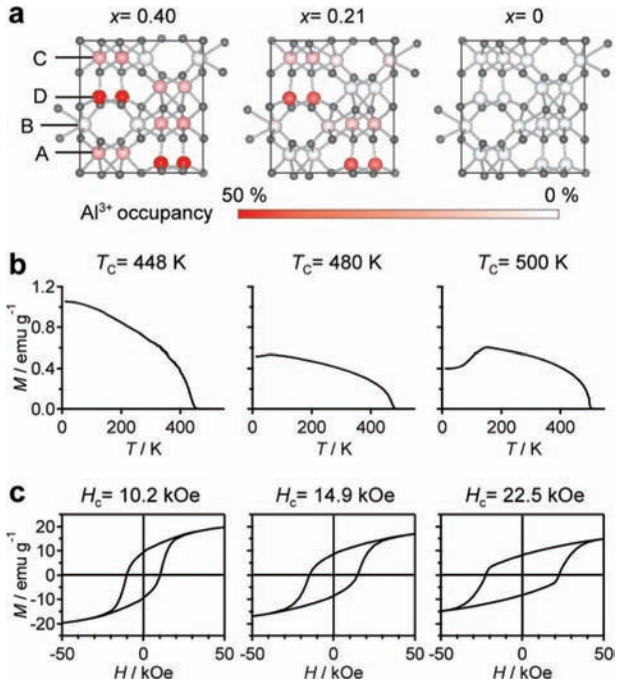

Figure 3. Distribution of Al substitutions and magnetic properties of ε-$Al_xFe_{2-x}O_3$ ($x = 0.40$, 0.21, and 0). (a) Degrees of Al substitution at each Fe site (A−D) described by the shade of red. (b) FCM curves for $x = 0.40$, 0.21, and 0 in the external magnetic field of 10 Oe. (c) Magnetization vs external field plots for $x = 0.40$, 0.21, and 0 at 300 K.

tie type low-temperature-grown GaAs photoconductive antennas were used, respectively. The sample was mounted on the sample holder, which was inserted between a set of paraboloidal mirrors. The electric fields of the transmitted THz pulse wave formed in the time domain were obtained by changing the delay time between the pump and the probe pulses. The absorption spectra of the THz waves were calculated by the following equation: (absorption) = $-10 \log |t(\omega)|^2$ (dB) ($t(\omega)$; complex amplitude transmittance). Samples were held in paper containers (8 mm × 8 mm × 8 mm). The fill ratios of the powder-form samples to the sample holder were as follows: 30% ($x = 0$), 26% ($x = 0.06$), 24% ($x = 0.09$), 29% ($x = 0.21$), 29% ($x = 0.30$), and 34% ($x = 0.40$). An absorption of 20 dB indicated that 99% of the introduced EM waves were absorbed, which is the target value for EM absorbers from an industrial point of view.

Results and Discussion

TEM images indicated that the nanoparticles have an average particle size between 25 and 50 nm (Figure 2 and Figure S2), and Rietveld analyses of the XRD patterns demonstrated that the materials in this series have an orthorhombic crystal structure in the $Pna2_1$ space group (Figure 2, Table S1, and Figure S2). This crystal structure has four nonequivalent Fe sites (A−D); that is, the coordination geometries of the A−C sites are octahedral [FeO_6], while that of the D site is tetrahedral [FeO_4]. For example, in the sample of $x = 0.21$, the degree of Al substitution of the D sites was 30%, whereas those of the A, B, and C sites were 0%, 3%, and 8%, respectively. Al ion predominantly occupied the D site because Al^{3+} (0.535 Å) has a smaller ionic radius than Fe^{3+} (0.645 Å),[21] and thus Al prefers the tetrahedral sites. The shade of red in Figure 3a depicts the degree of Al substitution. The lattice constants for these samples were systematically compressed as x increased (Table 1).

Table 2. Magnetic Properties of ε-$Al_xFe_{2-x}O_3$

x	T_C/K	H_c/kOe[a]	M_s/emu g^{-1}[a]
0	500	22.5	14.9
0.06	496	19.1	15.1
0.09	490	17.5	14.6
0.21	480	14.9	17.0
0.30	466	13.8	20.3
0.40	448	10.2	19.7

[a] Values measured at 300 K.

Figure 3b shows the field-cooled magnetization (FCM) curves for $x = 0.40$, 0.21, and 0 in an external magnetic field of 10 Oe, which indicated that the T_C values are 448, 480, and 500 K for $x = 0.40$, 0.21, and 0, respectively. Figure 3c plots the magnetization versus external magnetic field for $x = 0.40$, 0.21, and 0 at 300 K. The H_c values at 300 K were 10.2, 14.9, and 22.5 kOe for $x = 0.40$, 0.21, and 0, respectively. The saturation magnetization (M_s) values at 300 K in an applied magnetic field of 50 kOe were 19.7, 17.0, and 14.9 emu g^{-1} for $x = 0.40$, 0.21, and 0, respectively. Figure S3 shows the FCM curves and the magnetization versus external field at 300 K for the other compositional materials. Table 2 summarizes the magnetic properties.

The frequencies of the absorption peaks in the millimeter wave range for $x = 0.40$, 0.30, 0.21, 0.09, 0.06, and 0 were observed at 112, 125, 145, 162, 172, and 182 GHz, respectively (Figure 4). In the case of a ferromagnetic material with a uniaxial magnetic anisotropy, the direction of magnetization was restricted around the magnetic easy-axis. However, when an EM wave was irradiated to a ferromagnetic material, the magnetization precessed around the easy-axis and a natural resonance occurred. The f_r value is proportional to H_a. When the sample consisted of randomly oriented magnetic particles, the H_a value

(21) Shannon, R. D. *Acta Crystallogr., Sect. A* **1976**, *32*, 751–767.

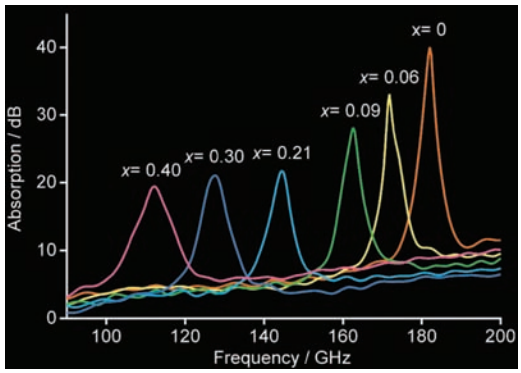

Figure 4. Millimeter wave absorption spectra of ε-$Al_xFe_{2-x}O_3$ for $x = 0.40$ (pink), $x = 0.30$ (blue), $x = 0.21$ (light blue), $x = 0.09$ (light green), $x = 0.06$ (yellow), and $x = 0$ (orange) measured by THz time domain spectroscopy.

is proportional to H_c. In fact, the observed f_r value increased as the H_c value increased.

Conclusions

In summary, we prepared a series of ε-$Al_xFe_{2-x}O_3$, which absorbs millimeter waves in the high frequency range. These f_r values are the highest values reported for any magnetic material. Such high frequencies can be achieved by a large H_a value of ε-Fe_2O_3, which has a large magnetic coercive field.[22−27] Because our materials are metal oxides, they are stable over long periods. Furthermore, because aluminum-substituted ε-iron oxide can be economically produced and does not harm the environment, the present new materials are advantageous for industrial applications of millimeter wave absorbers, including the body of a car, train, or airplane as well as the walls of an office, residence, or medical room.

Acknowledgment. The present research was supported in part by a Grant for the Global COE Program, "Chemistry Innovation through Cooperation of Science and Engineering", from the Ministry of Education, Culture, Sports, Science, and Technology, Japan, a Grant-in-Aid for Young Scientists (S) from Japan Society for the Promotion of Science, the Asahi Glass Foundation, Inamori Foundation, the Kurata Memorial Hitachi Science and Technology Foundation, and the Murata Science Foundation.

Supporting Information Available: Millimeter wave absorption measurements, TEM images, Rietveld analyses, and magnetic properties. This material is available free of charge via the Internet at http://pubs.acs.org.

JA807943V

(22) Jin, J.; Ohkoshi, S.; Hashimoto, K. *Adv. Mater.* **2004**, *16*, 48–51.
(23) Ohkoshi, S.; Sakurai, S.; Jin, J.; Hashimoto, K. *J. Appl. Phys.* **2005**, *97*, 10K312/1–10K312/3.
(24) Sakurai, S.; Jin, J.; Hashimoto, K.; Ohkoshi, S. *J. Phys. Soc. Jpn.* **2005**, *74*, 1946–1949.
(25) Kurmoo, M.; Rehspringer, J.; Hutlova, A.; D'Orleans, C.; Vilminot, S.; Estournes, C.; Niznansky, D. *Chem. Mater.* **2005**, *17*, 1106–1114.
(26) Gich, M.; Frontera, C.; Roig, A.; Taboada, E.; Molins, E.; Rechenberg, H. R.; Ardisson, J. D.; Macedo, W. A. A.; Ritter, C.; Hardy, V.; Sort, J.; Skumryev, V.; Nogues, J. *Chem. Mater.* **2006**, *18*, 3889–3897.
(27) Tronc, E.; Chanéac, C.; Jolivet, J. P. *J. Solid State Chem.* **1998**, *139*, 93–104.